Correlated stopping of Coulomb clusters in a dense jellium target

Claude Deutsch
Laboratoire de Physique des Gaz et des Plasmas, Bâtiment 212, Université Paris XI, 91405 Orsay, France
(Received 5 July 1994)

The strongly correlated stopping of N pointlike charges organized in clusters with a regular geometry is thoroughly investigated at high velocity as a linear and binary superposition of the stopping of a dicluster polarized with respect to the overall drift velocity. For $N \geq 3$, *a priori* unexpected N-body and collective behaviors are identified in terms of variations for the target electron density, cluster topology, charge distribution, and projectile velocity. The target is featured as a homogeneous and dense electron jellium quantified with the Wigner coupling parameters r_S. A corresponding dielectric function is taken in a plasmon pole approximation, allowing for a quasianalytic and transparent analysis. A recurring trend of this study is an enhanced stopping due to charge correlation, increasing rapidly with N. A noticeable counterexample is afforded by a regular N chain of charges flowing parallel to its velocity. As a rule, in most practical cases of interest, correlated charges within a few atomic interdistances can experience a stopping that is enhanced by orders of magnitudes relative to the isolated charge case, when stopped in a target at ordinary matter density, with initial kinetic energy in the tens of keV/amu range.

PACS number(s): 52.40.Mj, 34.50.Bw, 52.65.+z, 52.55.Mg

I. INTRODUCTION

The production and basic physical properties of atomic clusters are presently given an ever growing attention [1]. The interaction of clusters, in particular metallic or carbonlike, with cold or hot targets is envisioned either as an additional source of knowledge about clusters structure or as a powerful driver for compressing or processing the target material in order to achieve a prescribed result.

It is already a well documented fact that many regular and neutral cluster architectures may accommodate several additional positive or negative charges without any further fragmentation. This allows for an efficient linear acceleration process provided the gradient length of the given electric field remains larger than the cluster ion dimensions. These properties are now quite routinely probed and used in several acceleration experiments and projects [2] devoted to fullerenelike [3], carbonlike [4], or metallic [5] ions such as Au_n^{q+}. The acceleration and fragmentation in flight or in target is also a topic intensively investigated [6] for hydrogen clusters. The mass spectrum of the accelerated particles span a much wider range than that of normal atomic ions. This allows consideration of heavy cluster ions as a potential driver extending the capabilities of protons or heavy atomic ions to inertially drive a pellet to release thermonuclear energy arising from pressure-induced fusion reactions. Intense beams of those particles could thus provide a realization of some previous scenarios involving mesoscopic material such as dust or accelerated metallic plates [7].

The extrapolation to cluster ions beams of the concepts already developed for particle-driven inertial fusion through light or heavy atomic ions has been recently discussed [8]. The so-called direct-drive compression, elaborating at length on a huge hammerlike effect [9–11] arising from the enhanced correlated stopping (ECS) investigated at length in the present work, has already been demonstrated to be efficient when operated through cluster ions. The prospects for indirect drive through the production of x rays confined in a hohlraum around the thermonuclear pellet look even more promising [12].

The main goal of the present work is to lay the groundwork for a basic understanding of the strong interaction of the cluster ion debris resulting from an initial cluster ion impacting and fragmentating in the target outer layers. The fragmentation issues are not presently addressed. It is therefore taken for granted that the cluster ions get suddenly disrupted under impact, on a femtosecond time scale, through a kind of Coulomb-like explosion [13].

Moreover, we focus interest on situations where the initial impacting velocities are nearly fully transmitted to the ion debris. This hypothesis implies that the energy toll given in the Coulomb repulsion between ion debris remains negligible with respect to initial cluster kinetic energy. Such simplifying assumptions have been demonstrated to be compatible with a bona fide particle-driven compression [9] of a pellet containing a thermonuclear fuel. In such a case the interaction of ion debris with the target may be understood as a stopping process of many pointlike charges flowing in the vicinity of one another.

The complex interaction of a partially fragmented cluster ion stopped at low velocity in a dense electron jellium has been addressed by Abril and co-workers [14,15] through a dicluster correlation contribution averaged out over relative orientation [16]. Most cluster ion stopping calculation are performed assuming a quadratic dependence on the charge of ion debris. However, the difficult issues connected to including a cubic dependence (Barkaš effect) are currently under scrutiny by Mikkelsen and Sigmund [17].

Section II develops a linear formulation of Coulomb clusters built on pointlike charges in a dense electron jellium target based on the high velocity dicluster approach

proposed by Basbas and Ritchie [18]. The latter is extended to an N cluster through a straightforward binary superposition approximation. Ion-electron interactions within the target are treated by a plasma pole approximation [19], allowing for easy and nearly analytic technical manipulations, while retaining the essential physics involved. Section III demonstrates the strongly enhanced stopping derived from the considered formalism for an increasing number of correlated ion debris and how it depends on geometric configurations and sizes. In Sec. IV we give deeper attention to specific features such as those displayed by N chains. In Sec. V globally neutral Coulomb clusters are shown to display a nonzero stopping at finite size.

The incidences of uneven charge distributions are tackled in Sec. VI. Straggling is given proper attention in Sec. VII. Range-energy relationships are discussed in Sec. VIII and intriguing velocity dependences are demonstrated in Sec. IX. Concluding remarks are offered in Sec. X.

II. COULOMB CLUSTER STOPPING

Our technical starting point is a Coulomb cluster of nearby pointlike charges featuring ion debris resulting from an energetic fragmentation of a weakly ionized cluster ion accelerated toward a fully degenerate electron target. Each ion charge experiences a stopping force through Coulomb interaction with the jellium fluid. The corresponding physics is considered to be pretty well understood. For the past 20 years or so, a rather intense activity has also been given to formulating in various ways the stopping mechanisms of two charges flowing close to each other in a jellium or a harmoniclike collection of neutral atoms [13–15,17].

In this work, we emphasize a situation for energetic ion cluster fragments where the kinetic energy per nucleon E is ≥ 10 keV/amu, so the overall drift velocity after impact in the target remains at least two orders of magnitude above the transverse velocity due to ion-ion Coulomb repulsion (intercharge distance ≥ 1 a.u.). In such a case, ion stopping may well be addressed within a kind of Bohr-Bethe-Bohr formulation. For example, stopping within solid Li ($r_S=3.27a_0$) in this given velocity range, the stopping time will be $\sim 10^{-13}$–10^{-12} sec with a much slower ion-ion relative motion. Such a picture enables us to consider a frozen configuration of ion debris building up a kind of Coulomb cluster interacting mostly with degenerate target electrons. We shall restrict our attention to regular topologies with constant ion-ion nearest-neighbor distances. When this is not the case, it is rather easy to describe the actual situation through suitable averages of regular Coulomb clusters [9].

A. Stability

The correlated stopping of a cluster of closely related ion debris is expected to display an observable effect because the stopping time is expected to remain much shorter than a typical Coulomb repulsion time. The ratio of these two times is given by the ratio of the corresponding energies. The Coulomb cluster is therefore experiencing a kind of dynamic stability. Coulomb clusters are also likely to display static stability. Recently it has been shown that regular Coulomb clusters [20] may exhibit a negative binding energy where the target may be modeled as a rigid background of a neutralizing charged fluid within the framework of a strongly coupled one-component plasma. Such a modeling implies a total neglect of any dynamic interaction between flowing cluster fragments and the target ions. Such a drastic approximation is likely to be valid over a large part of the presently considered velocity range. Even without invoking a genuinely bound cluster structure, recent calculations have shown [21] that a cluster of ten ion charges arranged regularly on a circumference is barely disturbed by the target electrons as long as their velocity stays far below the cluster velocity.

B. Dicluster stopping

Here we briefly review the polarized stopping of a dicluster with interdistance $\mathbf{R}$ (see Fig. 1) between charges 1 and 2. We follow closely a recent presentation due to Basbas and Ritchie [18], developed within a three-dimensional framework in cylindrical coordinates about the velocity axis $\mathbf{v}$.

First, one immediately retrieves the isolated charge energy loss per unit length to target electronic excitations, given as (in a.u.)

$$S_p=\frac{e^2\omega_p^2}{v^2}\ln\left[\frac{2mv^2}{\hbar\omega_p}\right] \tag{1}$$

for ion cluster fragments with charge $Z_i=1$, velocity v, and the target plasma frequency $\omega_p=\sqrt{3}/r_S^{3/2}$, in terms of the Wigner coupling parameter $r_S=(\frac{4}{3}\pi n_e)^{-1/3}a_0$, where a_0 is the Bohr radius. m is the electron mass.

For a solid density Li target with $r_S=3.27a_0$, the electron number density will range from $n_e=2\times 10^{17}e$ cm^{-3} ($r_S=200a_0$) to $n_e=4.58\times 10^{28}e$ cm^{-3} ($r_S=0.0327a_0$), excluding the relativistic edge at $r_S\leq 0.01a_0$. The target medium is taken as a fully degenerate electron jellium in the so-called plasma pole approximation [18] with the dynamic dielectric function $\epsilon(k,\omega)$ explained as

$$\mathrm{Im}\left[-\frac{1}{\epsilon(k,\omega)}\right]=\frac{\pi\omega_p^2}{2\omega}\left[\delta(\omega-\omega_p)\theta(k_c-k)+\delta\left[\omega-\frac{\hbar k^2}{2m}\right]\theta(k-k_c)\right], \tag{2}$$

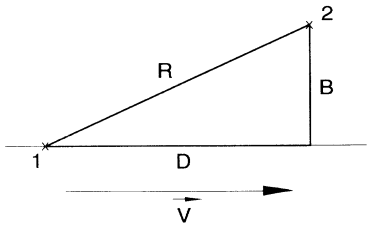

FIG. 1. Cylindrical coordinates along velocity for dicluster stopping with intercharges distance R.

The choice $k_c=(2m\omega_p/\hbar)^{1/2}$ allows the two δ functions to coincide at $k=k_c$ in the k-ω plane, depicted on Fig. 2. Approximation (2) corresponds to dashed curve on Fig. 2.

Working out the response theory up to the first-order Born approximation, according to Fig. 1 geometry, we can write down the dicluster energy loss in the form $(k^2=\kappa^2+\omega^2/v^2)$

$$S_c=\frac{2e^2}{\pi v^2}\int_0^\infty \kappa\, d\kappa \int_0^\infty \frac{\omega\, d\omega}{k^2}\mathrm{Im}\left[\frac{-1}{\epsilon(k,\omega)}\right] \times\left[Z_1^2+Z_2^2+2Z_1Z_2J_0(\kappa B)\times\cos\left[\frac{\omega D}{v}\right]\right] \equiv(Z_1^2+Z_2^2)S_p+2Z_1Z_2S_v(B,D)\ . \quad (3)$$

The right-hand side of Eq. (3) is straightforwardly interpreted as a superposition of isolated stopping contributions for particles 1 and 2 with a crossed term due to dynamic interferences between the two charges. Introducing Eq. (2) into Eq. (3) yields

$$S_v(B,D)=\frac{e^2\omega_p^2}{v^2}\left[\cos\left[\frac{\omega_p D}{v}\right]\int_0^{\kappa_c}\frac{\kappa J_0(\kappa B)}{k^2+\omega_p^2/v^2}d\kappa + \int_{k_c}^{k_2}\frac{dk}{k}\cos\left[\frac{\hbar k^2 D}{2mv}\right]J_0(QB)\right]\ , \quad (4)$$

where $Q^2=k^2-(\omega_k/v)^2$, $\kappa_c^2=k_c^2-\omega_p^2/v^2$, $\omega_k=\hbar k^2/2m$, $k_2=2mv/\hbar$, and $J_0(x)$ is the usual Bessel function.

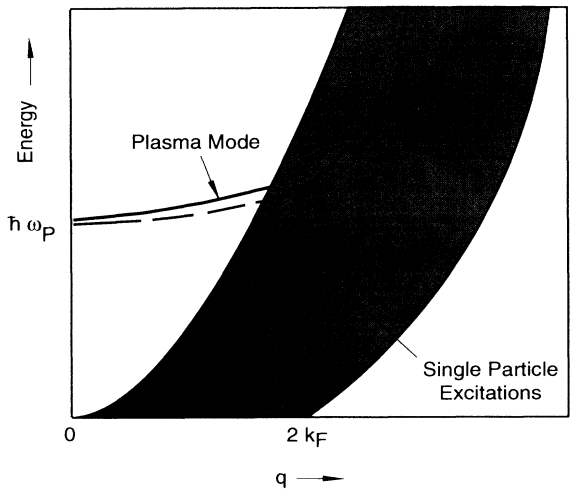

FIG. 2. Spectrum of excitation energies vs wave-vector transfer q for an interacting electron gas. The upper boundary of the single-particle excitations is $(\hbar^2/2m)[(k_F+q)^2-k_F^2]$ and the lower boundary is $(\hbar^2/2m)[(-k_F+q)^2-k_F^2]$. In the plasmon model, this spectrum is replaced by a single mode $\hbar\omega(q)$, indicated by the dashed line [after A. W. Overhauser, Phys. Rev. B 3, 1881 (1971)].

C. *N*-cluster stopping

Now, it is a straightforward matter to apply Eq. (4) to any selected (i,j) pair within a given configuration of N pointlike charges. The corresponding energy loss appears as a linear superposition of the dicluster one, given by

$$S_c=\left[\sum_i Z_i^2\right]S_p+2\sum_{1\le i<j\le N} Z_iZ_jS_v(B_{ij},D_{ij})\ , \quad (5)$$

in terms of the definitions (1) and (4). S_c is obviously bounded by the pointlike stopping of the coalesced charge $\sum_{i=1}^N Z_i$. A detailed study of the actual range in the coalesced limit has been given recently for a partially degenerate target within the random-phase approximation for dicluster stopping and for straggling as well [22].

As far as the presentation of numerical results in the sequel is concerned, it appears convenient to introduce the ratio of correlated to total stopping [see Eq. (5)] fulfilling

$$\mathcal{R}_1=2\sum_{1\le i<j\le N} Z_iZ_jS_v(B_{ij},D_{ij})S_c^{-1}<1-\frac{\sum_i Z_i^2}{\left[\sum_i Z_i\right]^2}\ . \quad (6)$$

An obviously related quantity of great interest is

$$\mathcal{R}_2=\frac{2\sum_{1\le i<j\le N} Z_iZ_jS_v(B_{ij},D_{ij})S_c^{-1}}{\sum_{i=1}^N Z_i^2S_p} =\frac{\mathcal{R}_1}{1-\mathcal{R}_1}\le\frac{\left[\sum_i Z_i\right]^2}{\sum_i Z_i^2}-1\ , \quad (7)$$

denoting the ratio of correlated to uncorrelated stopping.

Symmetric charge configurations with $Z_1=Z_2=\cdots=Z_N\equiv Z$ fulfill $\mathcal{R}_1\le 1-N^{-1}$ and $R_2\le N-1$. In this case, one has $0.666\le\sup(\mathcal{R}_1)\le 1$ with $3\le N\le\infty$. $\sup(\mathcal{R}_1)$ refers to the right-hand side of inequality (6). Selecting a highly asymmetric configuration with $Z_1=Z_2=\cdots=Z_{N-1}=1$ and $Z_{N=1}$, one witnesses $0.59\le\sup(\mathcal{R}_1)\le 0.75$ with $3\le N\le\infty$. As a consequence, as confirmed below, one is led to estimate symmetric configurations as those providing the highest correlated stopping.

Before detailing the numerical and physical content of expression (5) in the next section, it should be mentioned that we have intentionally left aside the important discussion about its validity when arbitrarily large Z_i values are introduced. Here we take the simple view that projectile charges are fixed during the stopping process and we push the present linear analysis to its limits in order to unravel the specific qualitative and semiquantitative features of correlated ion species in the high velocity range of present interest.

III. ENHANCED CORRELATED STOPPING

Referring to Eq. (5), the first and obvious manifestation of the ECS concerns the N dependence for a given spatial

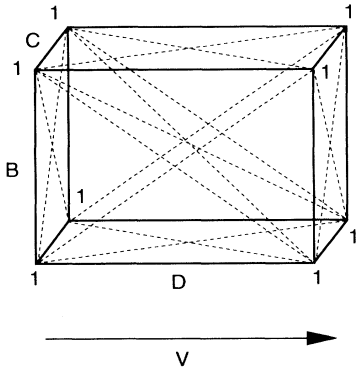

FIG. 3. Eight-cluster stopping in jellium target for unit charges located at vertices of a rectangular box.

charge configuration. In order to highlight the basic physics features of the present model, we first assume that every correlated charge flows with the same velocity. For instance, Fig. 3 depicts a regular distribution of eight pointlike charges with 28 charge-charge connections. Then if one displays step by step 15 charges on a cubic box with $B=C=D=2$ a.u., as in Fig. 4, one witnesses a rapid increase of the stopping per charge and of the correlation contribution featured by the ratio $\mathcal{R}_2$.

This mundane example demonstrates how efficient the charge correlation may be, even with a relatively reduced number of ion debris. The jellium density ($r_S=3.27a_0$) corresponds to a lithium blanket of a thermonuclear fusion pellet [9].

The next step in investigating the ECS is afforded by different charge configurations with the same N and charge connectivity (number of bonds at a given particle location). In Fig. 5 a boxlike arrangement is compared to lines of regularly spaced pointlike charges, flowing either along or transverse to an overall drift velocity. As intuitively anticipated, the compact boxlike topology displays a faster increase in stopping with N. Moreover, linear charge arrays transverse to velocity are more efficiently stopped than longitudinal ones.

This example makes it clear that, everything else being equal, the repartition of charges with respect to velocity is a significant parameter qualifying stopping performances. For instance, if one is looking for an efficient hammerlike pressure in a given target [9–11], one is led to prefer compact Coulomb clusters providing the shortest ranges, with the highest resulting rate of shock wave production.

It is also very important to investigate, for a given cluster geometry, the size dependence of its stopping capabilities in a given target. For that purpose, Fig. 6 features the cubic box depicted in Fig. 4 with a charge nearest-neighbor distance ranging from zero (coalesced) to 2.5 (in a.u.), at three target densities differing by order of magnitude. As expected, the stopping per charge steadily decays as the size increases, while the correlation ratio spans nearly all of its allowed range [Eq. (7)], including the upper bound $N-1$ at full coalescence. It also decreases rapidly and even goes down to zero at very small target electron correlation length $\sim 1.1 r_S^{1/2}$ [cf. Fig. 6(c) with $r_S=0.0327a_0$].

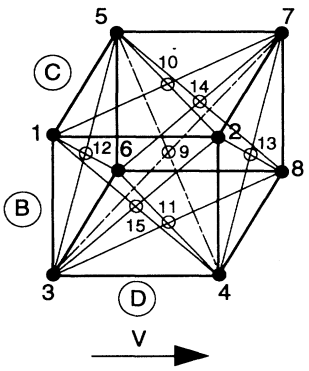

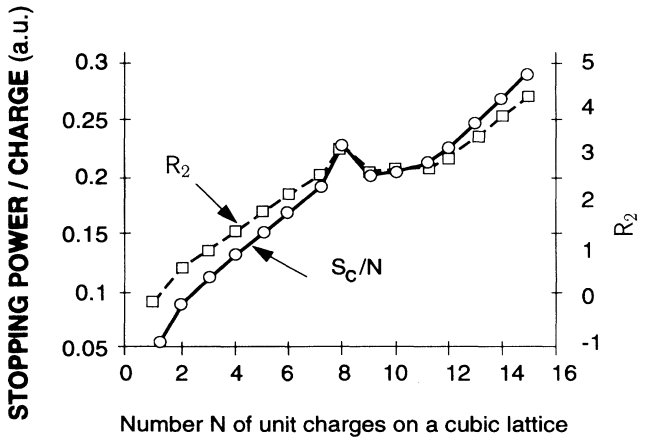

FIG. 4. Stopping per charges of $1\le N\le 15$ unit charges located at the vertices, center, and the face center of a cubic box $B\times C\times D$ with $B=C=D=2$ a.u. The overall drift velocity is $v=2.4$ a.u. $\mathcal{R}_2$ denotes the ratio (7). $D\|v$.

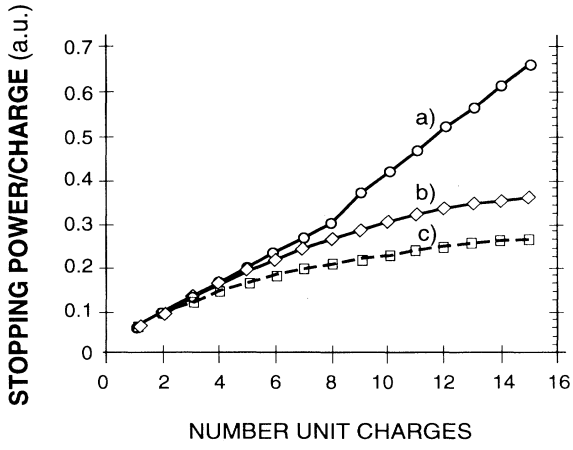

FIG. 5. Stopping per charges of $1\le N\le 15$ unit charges, distributed on three different arrangements. $v=2.4$ a.u. and $r_S=3.27a_0$. (a) Centered cubic box $B=C=D=1$ a.u. (b) N chain $B=1$ a.u.$\perp v$. (c) N chain $D=1$ a.u. $\|v$.

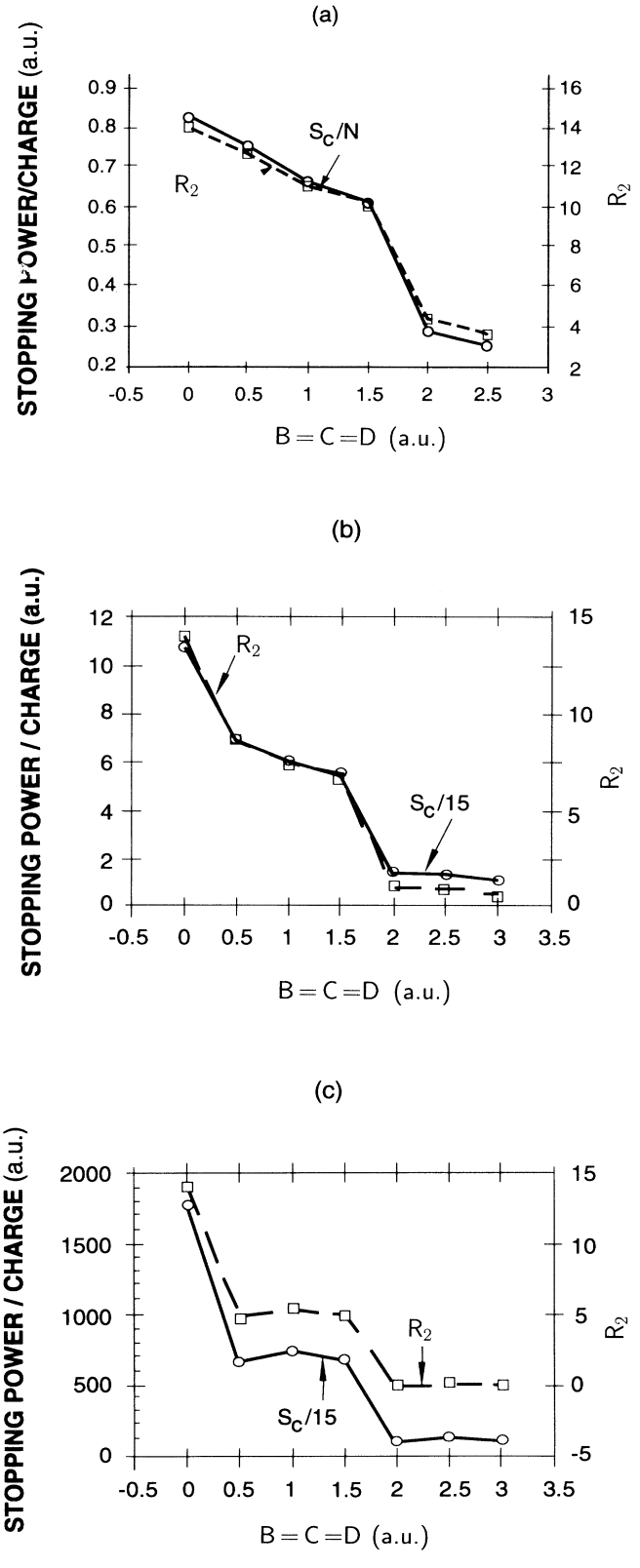

FIG. 6. Stopping per charges and correlation ratio $\mathcal{R}_2$ of 15 unit charges located at the vertices, center, and the faces on cubic boxes of various sizes. $D \| v$. (a) $r_S = 3.27a_0$ and $v = 2.4$ a.u. (b) $r_S = 24$ a.u. and $v = 0.327$. (c) $r_S = 0.0327a_0$ and $v = 43$ a.u.

IV. *N* CHAINS

Once generic trends of the ECS are identified, it is of special interest to focus attention on specific stopping features. Within the present formalism, the simulation of the behavior of large N chains with $N \gg 1$ is easily affordable. This allows us to contrast more effectively the stopping of N chains respectively parallel and transverse to **v**, already alluded to in Fig. 5. According to Eqs. (4) and (5), the oscillatory patterns, in particular, for N chains along velocity, are monitored by the ratio $\omega_p D/B$. Figure 7(a) corresponds to a value 0.1220, while Fig. 7(b) has 0.9763. In both situations, the longitudinal propagation exhibits oscillations and the transverse one shows a similar trend. After a rapid increase with N, the transverse N chains experience a well-behaved plateau behavior for the stopping per charge. At large N value,

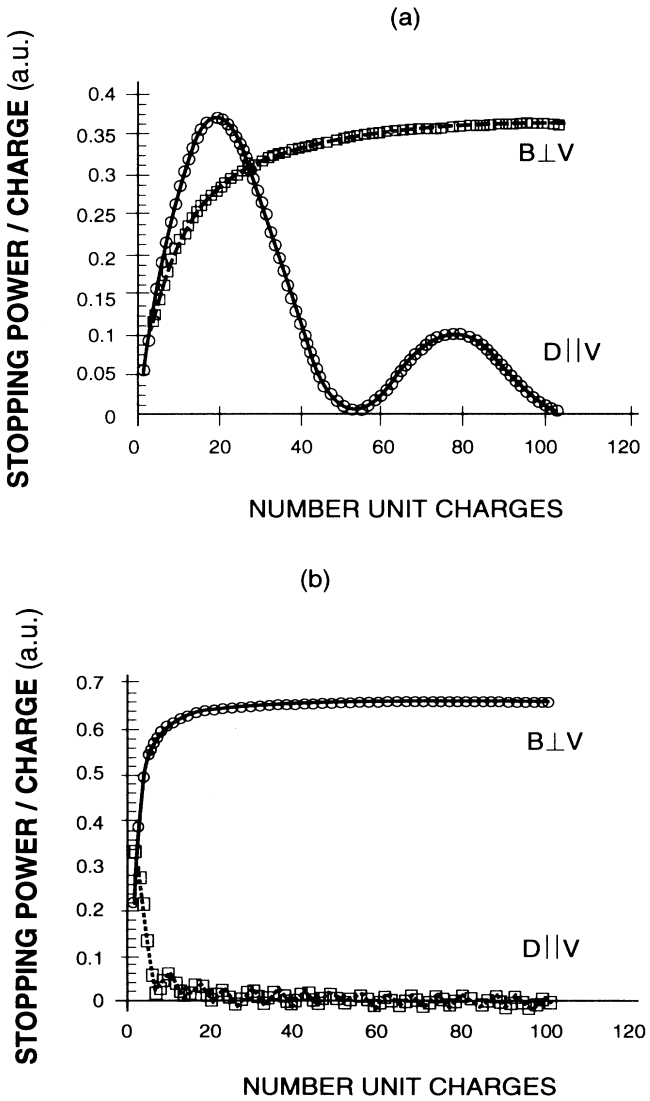

FIG. 7. N-chain stopping of unit charges in solid Li ($r_S = 3.27a_0$). (a) $v = 2.4$ a.u. and $B = D = 1$ a.u. (b) $v = 0.6$ a.u. and $B = 2$ a.u.

longitudinal chains obviously experience a strong and negative correlation contribution to stopping.

The remaining overall energy loss, while still positive, appears to arise only from a few particles. All other particles seem to experience a kind of surfing effect, with practically no stopping at all. On the other hand, the transverse N chains display a pattern where every charge contributes the same definite amount. In that case, every particle has to make its way, while keeping track of its neighbor through a strong and positive correlation contribution.

With a view toward future fusion applications, it is of interest to gain more insight about the promising behavior of the transverse propagation. In Fig. 8 we consider a target a little more dense than that discussed above ($r_S = 2.1446 a_0$) with a nearest-neighbor transverse distance of $B = 1$ a.u. In Fig. 8(a), we picture first an oblique propagation at $\pi/4$ relative to **v**. The profile in N of the stopping per charge appears to be strikingly similar to the pure transverse profile [Fig. 8(b)] with $D = 0$. Such a result is quite encouraging as far as matter compression is concerned. It demonstrates that only the pure longitudinal N-chain propagation with $B = 0$ might be deleterious in allowing a strongly reduced stopping efficiency and a resulting longer range in target. Actually, a closer scrutiny [22] of the plasmon pole approximation (2) shows that more damping has to be included in order to partially bridge a gap with an actual target, which indeed brings in a more efficient longitudinal stopping efficiency. In Figs. 8(a) and 8(b) the saturation plateau occurs for a correlated stopping higher than 50% of the total, as featured by the ratio $\mathcal{R}_1$.

It is also of theoretical interest to notice that a weak correlation contribution to stopping persists even for a very nearest-neighbor interdistance. In Fig. 9 we see that with $B = D = 100$ a.u., both transverse and longitudinal N chains still behave qualitatively as former ones, where $B = D = 1$ a.u. Of course, as expected, the value of the

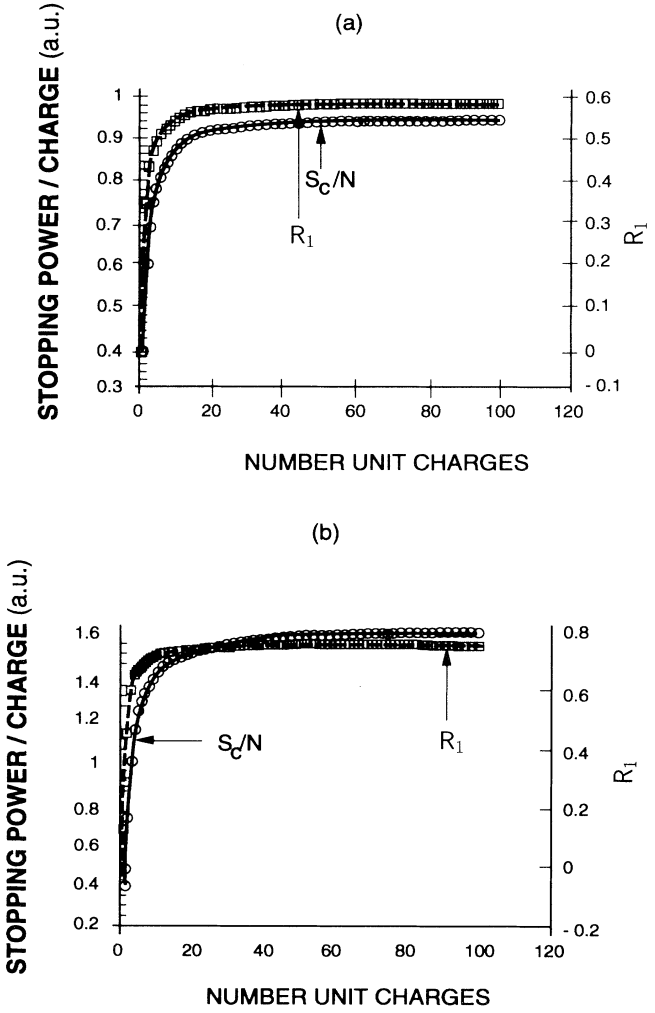

FIG. 8. N-chain stopping of unit charges in a dense jellium target ($r_S = 2.1446 a_0$). (a) $\pi/4$ propagation with $B = D = 1$ a.u. and $v = 1$ a.u. (b) Transverse propagation with $B = 1$ a.u. and $v = 1$ a.u.

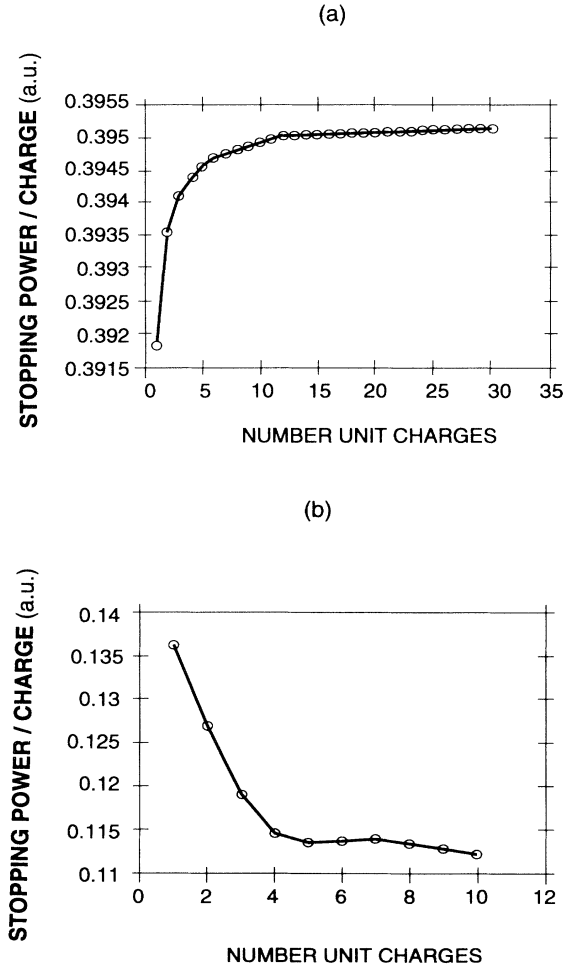

FIG. 9. Stopping N-chains unit charges with very large intercharge distances. (a) Transverse propagation with $B = 100$ a.u., $v = 1$ a.u., and $r_S = 2.1446 a_0$. (b) Parallel propagation with $D = 100$ a.u., $v = 1.2$ a.u., and $r_S = 3.27 a_0$.

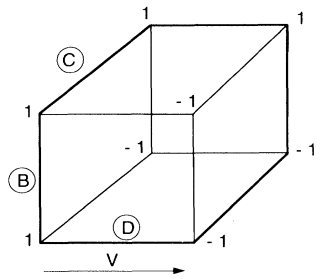

(a)

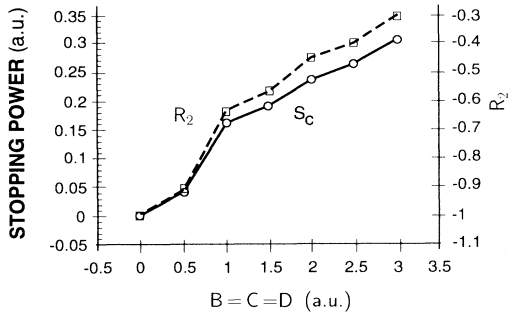

(b)

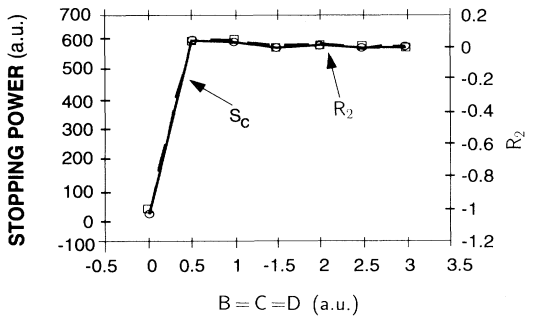

(c)

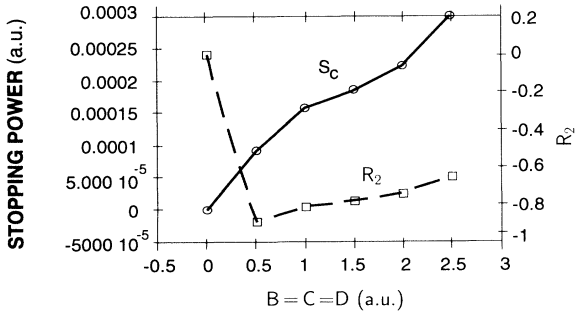

FIG. 10. Stopping of an overall charge neutral cubic box arrangement in terms of intercharges distance. (a) $v=2.4$ a.u. and $r_S=3.27a_0$. (b) $v=13$ a.u. and $r_S=0.0327a_0$. (c) $v=2.4$ a.u. and $r_S=32.7a_0$.

stopping per charge is now very close to the isolated charge value, especially in the transverse case. The interest of the comparison lies in the fact that for very small correlations, one witnesses a positive contribution for a transverse N chain and a negative contribution longitudinally.

V. OVERALL NEUTRAL COULOMB CLUSTERS

The flexibility and power of the unassuming expression (5) is demonstrated once more by the straightforward insight it allows for rather exotic charge configurations. In real experimental situations, it is not uncommon that due to charge fluctuations in target an excess of electrons can stick to a given ion debris.

It is also likely that the so-called convoy electrons may be dragged at same velocity **v** along ion debris. In such a case, one is confronted with a Coulomb cluster with pointlike (or nearly pointlike) charges of either sign. A rather obvious realization of such a situation within the present modeling may be pictured as a boxlike structure of positive and negative charges regularly spaced, as seen in Fig. 10(a), featuring a globally neutral but extended system of charges. In such a case, with geometric and dynamic parameters already used previously for one sign clusters, one observes a behavior opposite to that already seen. At vanishing interdistances, coalescence now reduces stopping to zero, while an increasing cluster size now causes the energy loss to increase. Of course, such an increase has to be bounded for very large interparticle distances. This is indeed confirmed in Fig. 10(b) for a very dense target ($r_S=0.0327a_0$) with a very short degenerate electron screening length, which thus clearly limits the stopping growth by the isolated charge value, with a vanishing ECS. Figure 10(c), with $r_S=32.7a_0(n_e\sim 4.6\times 10^{19}e\ \mathrm{cm}^{-3}$ in Li) illustrates the opposite case of a more dilute target with a slower ECS variation.

It is also of interest to notice that the propagation along **v** (Fig. 11) of N chains of alternate charges could decrease significantly the energy loss per charge below

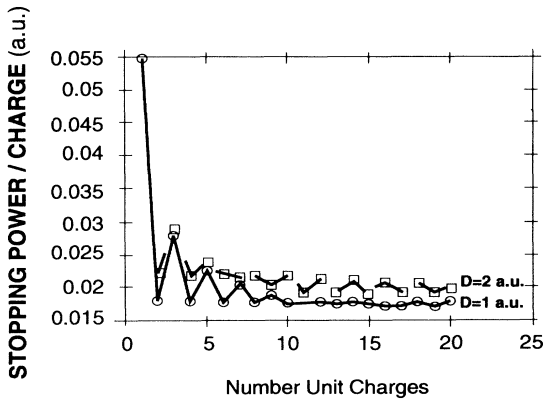

FIG. 11. Parallel stopping of N chains of alternate unit charges with $v=5$ a.u. and $r_S=2.1446a_0$ for two values of intercharges spacing.

the isolated charge value. In the case at hand, in Fig. 11, that reduction is by a factor of 3. Also, previous smooth oscillations (see Fig. 7, for instance) are now replaced by a sawtooth profile.

VI. UNEVEN CHARGE DISTRIBUTIONS

In order to make conspicuous the above displayed trends of the present formulation, we have purposefully restricted our discussion to Coulomb clusters with equal charges. Now, we release that limitation by considering a configuration of four charges located on vertices of a rectangle with one of its sides parallel to velocity [Figs. 12(a) and 12(b)]. In Fig. 12(a), we also put an extra charge at the center, while the charge Z of one vertex is changing. One thus witnesses a steady increase with Z of the stopping per charge, in view of the strong connectivity of this flat cluster. In Fig. 12(b) we investigate how a system of eight charges arranged in various repartitions at vertices and the center can influence the resulting energy loss, in terms of velocity.

According to the quadratic charge dependence of expression (5), the symmetric distribution $2+2+2+2$ displays the largest energy loss. Similar trends are observed in three dimensions.

Figure 13 displays a regular pyramidlike structure of five charges. Figures 13(a) and 13(b) now contrast the behavior of ECS, here featured by the correlation ratio $\mathcal{R}_1$. For five unit charges [Fig. 13(a)] a large portion of stopping is due to the ECS, while in the asymmetric case pictured in Fig. 13(b), with a quadrupled charge at the pyramid vertex, the ECS drops by at least a factor of 2. The ratio $\mathcal{R}_3$ now pertains to the ratio of the largest charge stopping relative to total. It is a striking feature that in contradistinction to other quantities, the largest charge stopping remains nearly constant with increasing velocity.

Similar trends are displayed by cubic clusters of unit charges centered with a much higher one, as shown in Fig. 14. The cubic box centered with a charge 8 at its center [Fig. 14(a)] exhibits a behavior very close indeed to that in Fig. 13(b), but extended to a much larger velocity range. On the other hand, the neutral combination $8\times1-8$ featured by Fig. 14(b) also emphasizes the specific features of an overall Coulomb cluster, already obtained in Sec. V. As a net result, when the cluster size increases, its energy loss reduces to that of the largest charge. Those specific behaviors would well introduce useful simplifications in the complex treatment of real experimental situations.

VII. STRAGGLING

Up to now, it has been implicitly assumed that every ion debris flows in a target at the same velocity **v**. Here we intend to remove such a restriction by investigating the quantitative significance of energy straggling. The corresponding analysis parallels that given in Sec. II for the stopping power.

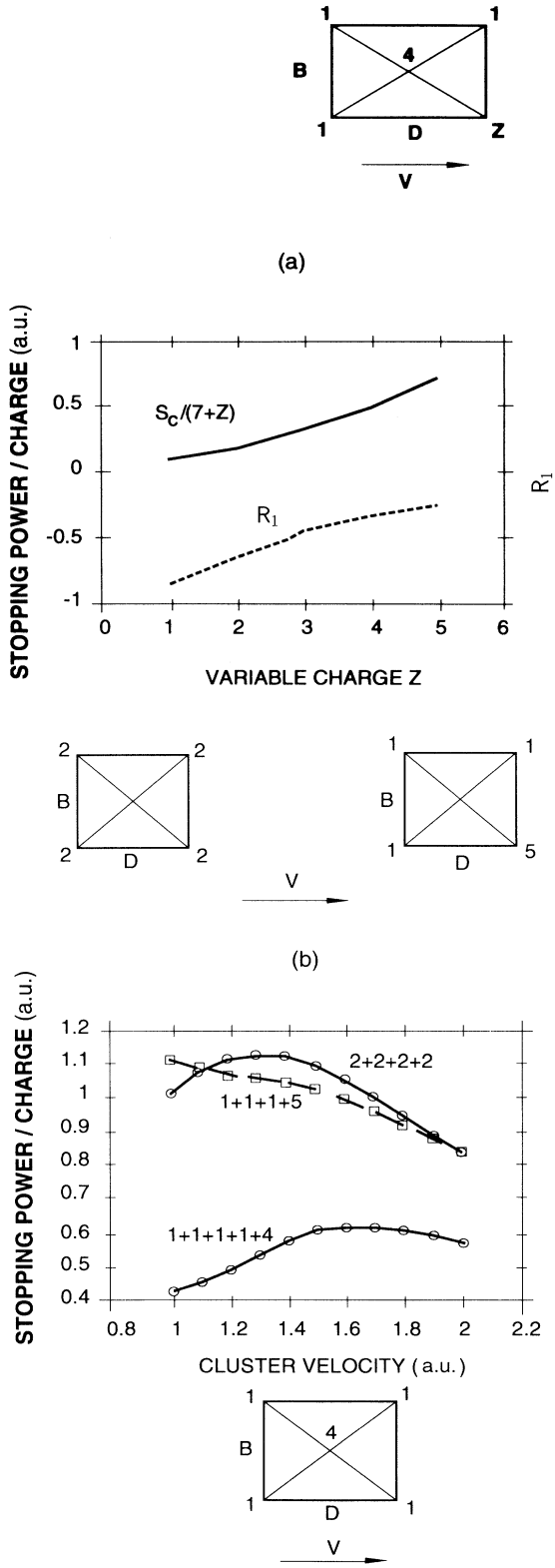

FIG. 12. (a) Stopping per charge of several charge distributions $1+1+1+Z+4$ at the vertices and the center of a square $B=D=2$ a.u. with $v=1$ a.u. and $r_S=2.1446a_0$. (b) Stopping squares $\|v$ with total charge 8 in jellium ($r_S=2.1446a_0$). $B=D=2$ a.u.

Starting with correlated dicluster straggling one has (see Fig. 1)

$$\Omega_{ij}\equiv(Z_1^2+Z2)\Omega_S^2+2Z_1Z_2\Omega_v^2$$
$$=\frac{2e^2}{\pi v^2}\int_0^\infty \kappa\,d\kappa\int_0^\infty \frac{\omega^2 d\omega}{k^2}\mathrm{Im}\left[-\frac{1}{\epsilon(k,\omega)}\right]$$
$$\times\left[Z_1^2+Z_2^2+2Z_1Z_2J_0(\kappa B)\times\cos\left[\frac{\omega D}{v}\right]\right], \quad (8)$$

where, as in Sec. II, $k^2=\kappa^2+\omega^2/v^2$. The expression on the right-hand side of (8) corresponds to one moment higher in ω relative to the stopping expression (3). In Eq. (8) the isolated particle contribution reads

$$\Omega_S^2=\frac{e^2\omega_p^3}{v^2}\left[\frac{1}{2}\ln\left[\frac{2mv^2}{\hbar\omega_p}\right]+\frac{mv^2}{\hbar\omega_p}-\frac{1}{2}\right], \quad (9)$$

while the correlated part is

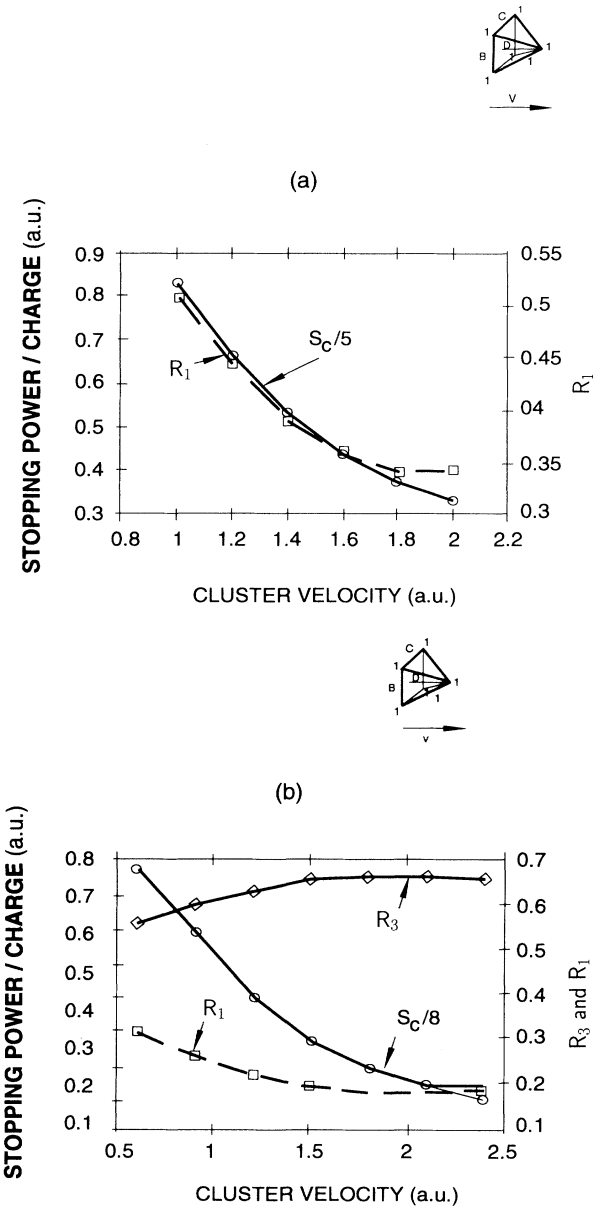

FIG. 13. Stopping per charge of a pyramid distribution with $B=C=D=2$ a.u. in terms of velocity. $D\|v$. (a) Five unit charges and $r_S=2.09a_0$ (Au). (b) Charge distribution $4\times1+4$ and $r_S=3.27a_0$ (Li).

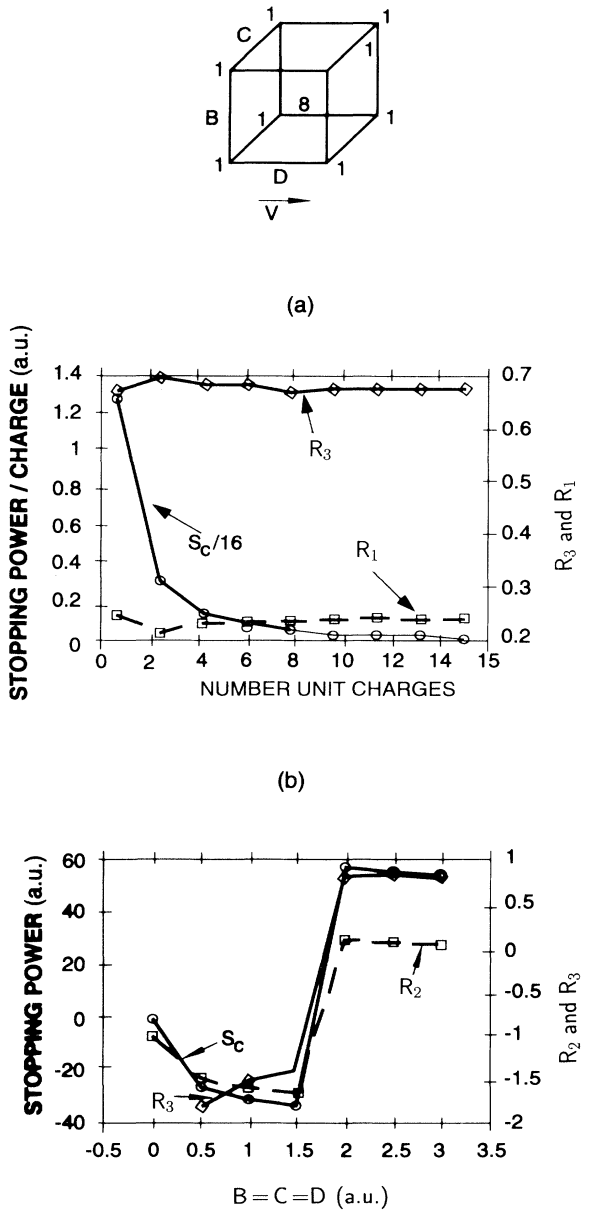

FIG. 14. Stopping of centered cubic box. $D\|v$. (a) $8\times1+8$, $B=C=D=2$ a.u., and $r_S=3.27a_0$ in terms of velocity. (b) $8\times1-8$, $v=24$ a.u., and $r_S=0.327a_0$ in terms of $B=C=D$.

$$\Omega_v^2=\frac{e^2\omega_p^3}{v^2}\left[\cos\left[\frac{\omega_p D}{v}\right]\int_0^{\kappa_c}\frac{\kappa J_0(\kappa B)d\kappa}{k^2+\frac{\omega_p^2}{v^2}}+\frac{\hbar}{2m\omega_p}\int_{k_c}^{k_2}dk\,k\cos\left[\frac{\hbar k^2 D}{2mv}\right]J_0(QB)\right], \tag{10}$$

with Sec. II notations. As above, the extension to a Coulomb cluster of N particles is now straightforward. Equation (5) for stopping is therefore paralleled with

$$\Omega_c=\left[\sum_i Z_i^2\right]\Omega_S^2+2\sum_{1\le i\le j\le N} Z_i Z_j \Omega_v^2(B_{ij},D_{ij}) \tag{11}$$

for straggling. In Fig. 15 we contrast expressions (5) for stopping and (11) for straggling by considering a distribution of four unit charges at the vertices of a rectangular tetrahedron. The overall behaviors are pretty similar when the cluster size increases. However, stopping is quantitatively more important, which gives some ground to the neglect of straggling in the polarized picture advocated here. Also, the correlation enhancement seems a bit less effective for straggling.

Switching to a cubic box with eight charges at vertices, Fig. 16(a) displays straggling variations in terms of velocity, while Fig. 16(b) features the effects of an increasing transverse size with respect to velocity. Again, those behaviors are close to their corresponding stopping counterparts. From the straggling quantity rewritten as $\langle \Delta E^2 \rangle$ and the stopping power dE/dx, one obtains the uncertainty on the interchange distance

$$\langle \Delta R^2 \rangle^{1/2} \approx \frac{\langle \Delta E^2 \rangle^{1/2}}{dE/dx},$$

which may account for inflight deformations of a given charge configuration.

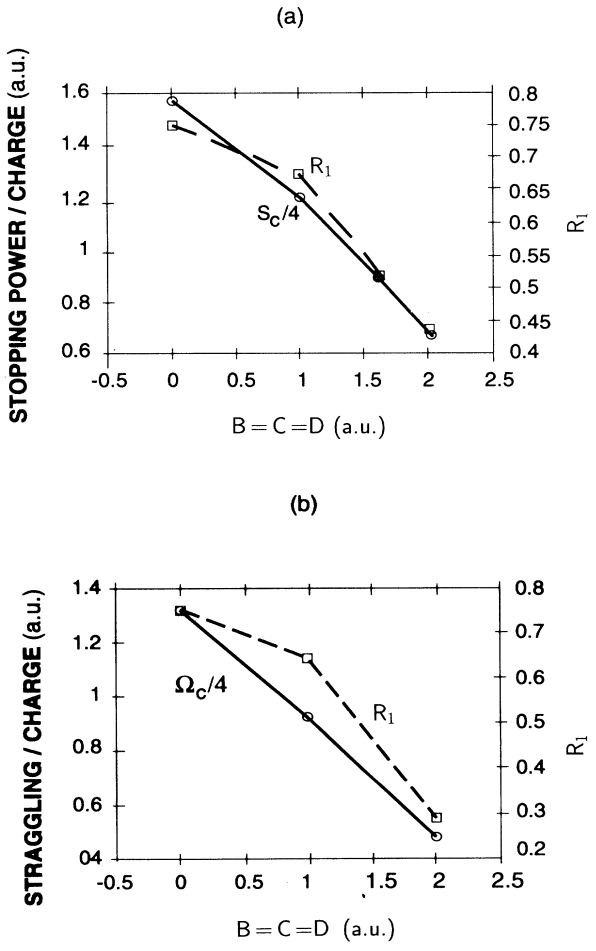

FIG. 15. (a) Stopping per charge of four unit charges at the vertices of a rectangular tetrahedron, $v=1$ a.u., and $r_S=2.1446a_0$ in terms of $B=C=D$. $D\|v$. (b) Same as in (a) for straggling.

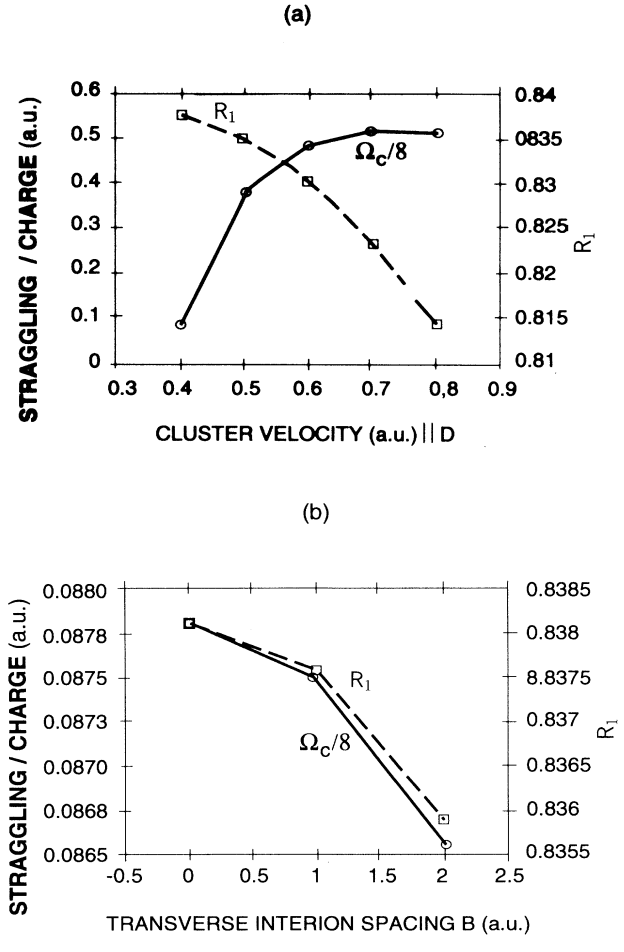

FIG. 16. Straggling per charge of cubic boxes bearing eight unit charges in Li targets ($r_S=3.27a_0$). (a) $B=C=D=1$ a.u. in terms of v. (b) $v=0.4$ a.u. and $C=D=1$ a.u. in terms of B.

VIII. RANGE-ENERGY RELATIONSHIPS

The ECS, amply documented in most of the previously considered stopping situations, should lead to much shorter stopping ranges in a target. With a view toward furtner compression of dense matter through intense beams of cluster ions, we picture in Fig. 17 (in physical units of practical interest) several range-energy relationships for dense jellium targets pertaining to the same cubic arrangement of eight unit charges and to several ma-

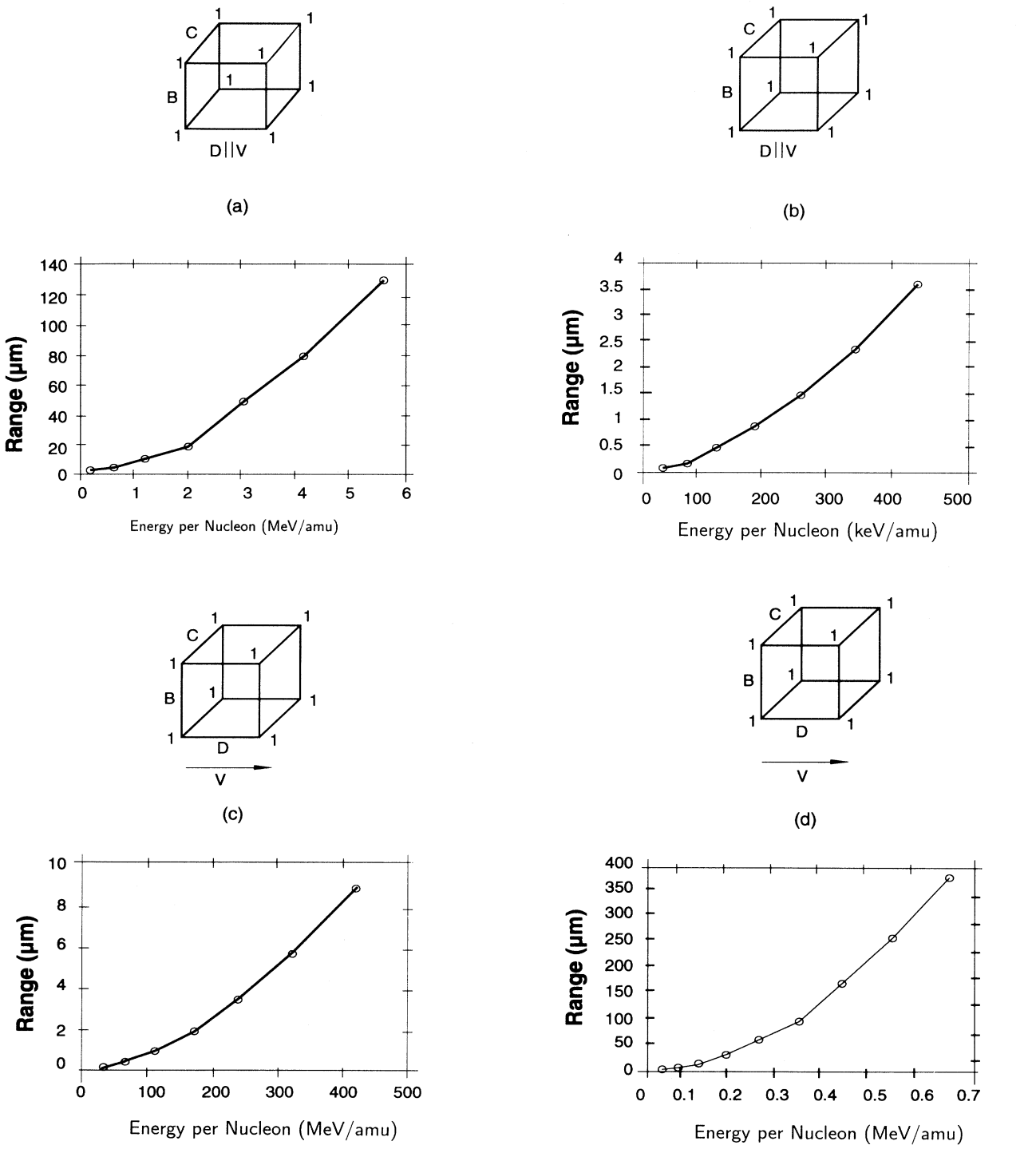

FIG. 17. Range energy relationships for cubic boxes with $B=C=D=2$ a.u. accommodating eight unit charges at vertices. $D\|v$. (a) $r_S=2.09a_0$ and v (3→15 a.u.). (b) $r_S=3.1a_0$ and v (0.6→4.1 a.u.). (c) $r_S=4.5a_0$ and v (0.6→4.1 a.u.). (d) $r_S=14.3889a_0$ and v (1.1→5.1 a.u.).

terials of potential interest as the convertor of the beam kinetic energy into hard photons (x rays). Qualitative results depicted in Fig. 17 look similar to those pertaining to atomic beams. However, as expected, the cluster ranges are shorter by an order of magnitude at the same projectile energy per nucleon. The given energy range (a few hundreds of keV/amu) is affordable on many tandem Van de Graaff linear accelerating structures, when adapted to deliver cluster ion beams.

IX. VELOCITY DEPENDENCE

Despite that the stopping dependence on velocity has already been met several times, it appears instructive to investigate more thoroughly some specific and unexpected trends. In particular, an interplay between v and r_S may unravel new features. The stopping of eight unit charges on a cubic box is shown in Fig. 18, in a rather low density target ($r_S = 6.678a_0$). Figure 18(a) exhibits at moderate v values (≤ 3.5 a.u.), a behavior $\sim v^{-2}$ close to a Bethe-like decay, with a corresponding correlation decay. However, at higher velocity [Fig. 18(b)], one observes a nearly constant correlation ratio $\mathcal{R}_2$, while stopping itself remains Bethe-like.

The relative increase with v of the correlation contribution stopping is expected on several grounds. Moreover, the interplay of v and r_S in very dense targets can lead to even more intriguing results. In Fig. 19 we consider a

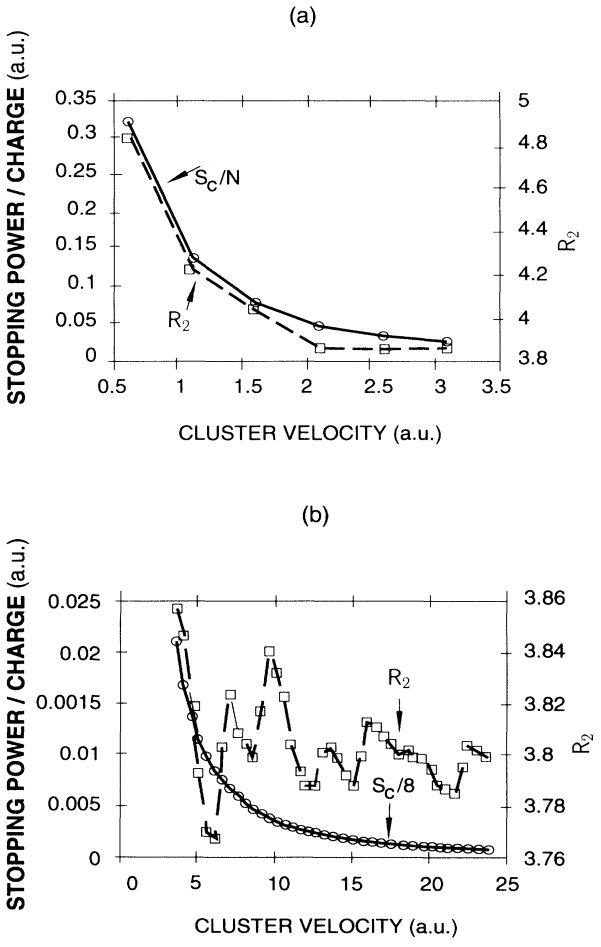

FIG. 18. Stopping per change in terms of velocity for a cubic box $B = C = D = 2$ a.u. with eight unit charges. $r_S = 6.678a_0$. (a) $0.5 \leq v \leq 3.5$ a.u. (b) $3.5 \leq v \leq 25$ a.u.

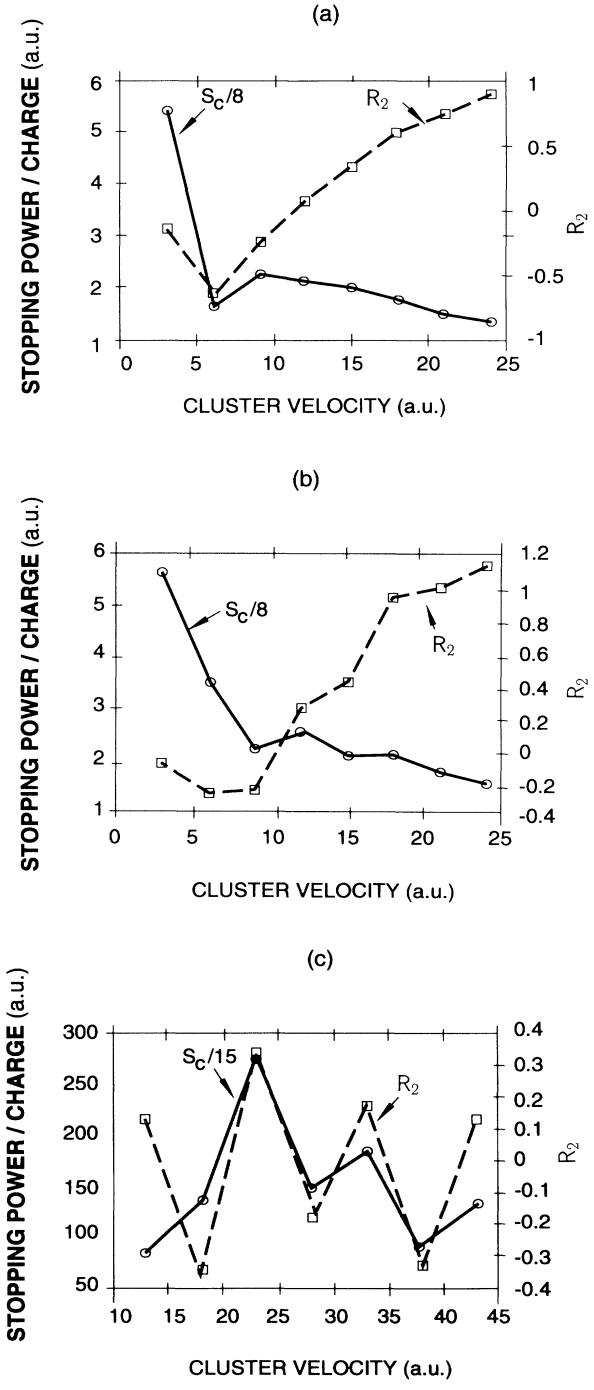

FIG. 19. Velocity dependence of stopping per charge of cubic distributions $B = C = D = 2$ a.u. of unit charges. $D \| v$. (a) $N = 8$ and $r_S = 0.327a_0$. (b) $N = 15$ and $r_S = 0.327a_0$. (c) $N = 15$ and $r_S = 0.0327a_0$.

target with $r_S = 0.327 a_0$ ($n_e = 4.5 \times 10^{25} e$ cm^{-3} in a target), a cubic arrangement of eight unit charges [Fig. 19(a)], and a face centered cubic arrangement of 15 charges [Fig. 19(b)], with $v \leq 25$ a.u.

Here, again, $\mathcal{R}_2$ increases significantly at high velocity. It displays a minimum for $5 \leq v \leq 10$ a.u., which turns slightly negative for the face centered arrangement [Fig. 19(b)]. However, in both cases stopping decay is essentially patterned through a two-slope process. A rapid decrease at $v \leq 10$ a.u. is followed by a much smoother one.

Even more exotic behaviors are seen in Fig. 19(c) for a cubic arrangement of 15 charges stopped in an even more dense target ($r_S = 0.0327 a_0$). Then, one witnesses practically no stopping decay at all with increasing v. Both total stopping and correlation stopping oscillate strongly at any v value. $\mathcal{R}_2$ features as many negative contributions as positive ones, although the geometry and the size of the considered Coulomb cluster do not change at all.

X. CONCLUDING REMARKS

We have seen how rich and diverse the physics of the stopping of Coulomb clusters in a jellium target is. In most situations of potential experimental interest, correlation among ion debris is expected to bring in a very strong stopping enhancement. The latter essentially depends on size, topological arrangement of particle locations, and charge distributions as well. The most symmetric ones are the most effective.

The very simple N-body model based on Eqs. (5) and (11) is actually full of unexpected features. Among them the very intriguing negative correlation brought about by a longitudinal propagation of a linear N chain parallel to its velocity should be addressed further. Also, the increasing correlation contribution with velocity to the stopping has to be given more scrutiny. The above studies make it clear that a most efficient target compression should be achieved through compact arrangements of pointlike charges. At a conceptual level, it should be appreciated that the present model allows for a rather pedestrian approach to the difficult issues of the interaction physics based on non-point-like objects, as highlighted by the stopping increasing with the size of a globally neutral Coulomb cluster.

Obviously several points have been left for further endeavor. They include Z^3 contributions, the introduction of relative angular averages to bridge the gap with available low velocity stopping results, and also a suitable in-flight charge evolution during the cluster penetration in target.

ACKNOWLEDGMENT

The Laboratoire de Physique des Gaz et des Plasmas is Unité Associé au Centre National de la Recherche Scientifique.

[1] See W. A. De Heer, Rev. Mod. Phys. **65**, 611 (1993), for a recent introduction to metallic clusters.
[2] P. Attal, S. Della-Negra, D. Gardès, J. D. Larson, Y. Le Beyec, R. Vienet-Lequé, and B. Waast, Nucl. Instrum. Methods A **238**, 293 (1993).
[3] S. Della-Negra, A. Brunelle, Y. Le Beyec, J. M. Curaudeau, J. P. Mouffron, B. Waast, B. V. R. Sundquist, and E. Parilis, Nucl. Instrum. Methods B **74**, 453 (1993).
[4] K. Boussofiane-Baudin, A. Brunelle, P. Chaurand, J. Depauw, S. Della-Negra, P. Håkanson, and Y. Le Beyec, Int. J. Mass Spectrom. Ion Processes **130**, 73 (1994).
[5] Ch. Schoppmann, P. Wohlfart, D. Brandl, M. Sauer, Ch. Tomaschko, H. Voit, K. Boussofiane, A. Brunelle, P. Chaurand, J. Depauw, S. Della-Negra, P. Håkanson, and Y. Le Beyec, Nucl. Instrum. Methods B **82**, 156 (1993).
[6] M. Farizon, N. V. De Castro Farcia, B. Farizon-Mazuy, and M. J. Gaillard, Phys. Rev. A **145**, 179 (1992).
[7] F. Winterberg, Z. Phys. A **296**, 3 (1980); T. Yabe and T. Mochizuki, Jpn. J. Appl. Phys. **22**, L262 (1983).
[8] C. Deutsch, Laser Part. Beam **8**, 541 (1990); **10**, 355 (1992).
[9] C. Deutsch and N. A. Tahir, Phys. Fluids B **4**, 3735 (1992); Nuovo Cimento **106A**, 1811 (1993).
[10] E. Nardi, Z. Zinamon, and D. Ben-Hamu, Nuovo Cimento **106A**, 1839 (1993).
[11] S. Eliezer, J. M. Martinez-Val, and C. Deutsch, Laser Part. Beam (to be published).
[12] N. A. Tahir, D. H. H. Hoffmann, J. A. Maruhn, and C. Deutsch, Nucl. Instrum. Methods B **88**, 127 (1994), and (unpublished).
[13] D. Kella, M. Algranati, H. Feldman, O. Heher, H. Kovner, E. Malkin, E. Miklazky, R. Naaman, D. Zajfman, J. Zajfman, and Z. Vager, Nucl. Instrum. Methods A **329**, 440 (1993).
[14] I. Abril, M. Vičanek, A. Gras-Marti, and N. R. Arista, Nucl. Instrum. Methods B **67**, 56 (1992).
[15] M. Vičanek, I. Abril, N. R. Arista, and A. Gras-Marti, Phys. Rev. A **46**, 5745 (1992).
[16] N. R. Arista and A. Gras-Marti, J. Phys. Condens. Matter **3**, 7931 (1991).
[17] H. H. Mikkelsen and P. Sigmund (unpublished).
[18] G. Basbas and R. H. Ritchie, Phys. Rev. A **25**, 1943 (1980) and references cited therein.
[19] A. W. Overhauser, Phys. Rev. B **3**, 1888 (1971).
[20] K. Tsuruta and S. Ichimaru, Phys. Rev. A **48**, 1339 (1993).
[21] A. Bret, Ph.D. thesis, Université Paris XI, Orsay, 1994; Nucl. Instrum. Methods B **88**, 107 (1994).
[22] A. Bret and C. Deutsch, Phys. Rev. E **47**, 1276 (1993); **48**, 2989 (1993).